

# Exploiting Short Block and Concatenated Codes for Reliable Communications within the Coexistence of 5G-NR-U and WiFi

M. Moazam Azeem, *Member, IEEE*, Raouf Abozariba, *Member, IEEE* and A. Taufiq Asyhari, *Senior Member, IEEE*

**Abstract**—Unlicensed spectrum offers opportunities for cellular mobile network operators, where traffic can be offloaded from licensed to unlicensed bands. Modern heterogeneous technologies such as 5G New Radio (NR) and WiFi can simultaneously operate on ISM and UNII bands under strict coexistence rules. While satisfying harmonious coexistence has largely been studied in LTE/4G, an emerging issue for future deployment is to reduce latency and to guarantee reliable communications, in the direction of achieving URLLC. This work mainly focuses on the critical issues arising in the coexistence of Listen Before Talk (LBT) systems, sharing common infrastructure of 5G NR-U and WiFi when operating under imperfect energy detection sensing. We consider the application of short, concatenated and product erasure correcting codes to recover missing data in LBT-based systems due to collisions. The goal is to enhance spectrum utilization with reduced delay and to achieve reliable communications under LBT and various sensing impairments, with code parameters such as block length, rate and minimum distance. By means of concatenation, we construct a series of sophisticated erasure block codes with less decoding complexity using Tanner Graph based decoding. Furthermore, we develop an analytical model to derive a closed-form expression using Gaussian approximation of spectrum utilization efficiency. The efficiency achieved using short, concatenated and product block codes is compared with the various low-density parity-check (LDPC) correcting ensembles under various levels of user activities, built by two state Gilbert-Elliott model. We provide detailed comparisons in respect of global throughput and failure probability of codes under varied number of coexisting users. Our results show that the proposed codes can achieve at least 20% higher efficiency at 0.1 false alarm probability and 30% less failure probability under high contention scenarios.

**Index Terms**—Unlicensed spectrum, Listen Before Talk (LBT), 5G New Radio Unlicensed (5G-NR-U), WiFi, erasure correcting codes, URLLC.

## I. INTRODUCTION

**N**EXT generation cellular network are expected to support end-user applications with heterogeneous quality requirements. In the context of IMT-2020 standards, the International Telecommunications Union (ITU) specified three main use cases as part of the future networks, namely ultra-reliable and low latency communication (URLLC), enhanced mobile broadband (eMBB), and massive machine-type communication (mMTC) [1]. These use cases need more spectrum to

meet the stringent demands. To expand the use of 5G cellular networks, involving unlicensed spectrum, 3GPP first targeted Unlicensed National Information Infrastructure (UNII) at 5 GHz and 6 GHz bands. Cellular operations can be performed over unlicensed bands with the requirement to satisfy spectrum regulations. The specifications for 5G NR-U [2] are introduced in the third generation partnership project (3GPP) release 16 [3] where it was noted that 5G NR-U is an extension of 4G Long Term Evolution (LTE) Licensed Assisted Access (LAA) standards introduced in 3GPP release 13. 5G NR-U can operate in three different deployment modes. The first mode is carrier aggregation that is based on LTE-LAA, where unlicensed spectrum is used to enhance downstream capacity for user plane traffic and licensed spectrum is used for control plane communications [4]. The second mode is dual connectivity that is based on extended LAA (eLAA) and supports both downstream and upstream for user plane traffic. The third mode is standalone where 3GPP defined that the user and control plane traffic can be transported over an unlicensed spectrum.

The standalone mode of 5G NR-U eliminates any dependency on the licensed network and can be implemented by any private enterprise, network system integrator or service provider. This opens a gateway for private 5G deployment that will support consumer demand and Industry 4.0 applications, fulfilling the criteria of low latency, higher bandwidth to densely populated areas. The carrier aggregation and dual connectivity modes operate in 5 GHz bands, while the NR-U standalone mode operates using sub 7 GHz and high-band spectrum ranging from 57-71 GHz. The major concern when 5G NR-U operates in a highly saturated 5 GHz band is to guarantee harmonious coexistence with other networks such as WiFi [5]. The addition of 5G NR Radio Access Network (RAN) should not create any interference to the existing WiFi system [6], [7]. While 5G NR-U uses the 5G-NR physical layer (PHY), it also benefits from the medium access control (MAC) layer protocols evolution where the channel access schemes are modified to operate with existing WiFi protocols. 5G NR-U uses similar contention-based protocol, LBT, that is already implemented in the current IEEE 802.11 standard to guarantee equal access to available channels and subbands [8], [9]. Although this mode of operation might limit some 5G-NR benefits, there are opportunities for higher spectral efficiencies and URLLC when using less congested new frequencies, e.g., 5.925-7.125 GHz frequency range that is available in

M. Moazam Azeem is with the College of Science and Engineering, Qatar University, Qatar (email: moazam@qu.edu.qa). Raouf Abozariba and A. Taufiq Asyhari are with the School of Computing and Digital Technology, Birmingham City University, UK (email: r.abozariba@ieee.org, taufiq-a@ieee.org)

the European Union, the United States and South Korea for unlicensed devices.

NR-U can also operate in CAT4 LBT where channels can be accessed following Carrier Sensing Multiple Access / Collision Avoidance (CSMA/CA) procedure. However, sensing techniques used in LBT such as energy detection and matched filter detection are commonly affected by two dominant impairments, namely, false alarm and non-detection probabilities. The former type leads to missed opportunities that can result in inefficient spectrum usage, while the second can lead to harmful interference. In addition, undetected hidden nodes can result in harmful interference, which in turn translates into collisions. In order to recover the data lost during the aforementioned collisions, the active user, who is transmitting data, could send an acknowledgement for the re-transmission of missing data packets. In this case, the active user needs a feedback channel and has to find an additional resource for re-transmission (channels, or another time slot). This can introduce excessive delays and the need for additional spectrum resources. Therefore, there is a pressing need to develop an alternative method of recovering the lost data without acknowledgement and without re-transmission within the coexistence of 5G NR-U and WiFi sharing a common infrastructure.

Our approach is to use short binary codes, such as Hamming, Golay, BCH, concatenated and product codes, with lower delay and complexity constraints rather than using very long codes with higher decoding complexity such as LDPC codes. We then compare the performance of short erasure correcting codes with that of long codes and product or concatenated codes. Our research is motivated by the fact that short codes and concatenated codes can in some cases significantly reduce the delay due to lower decoding complexity. Furthermore, the properties and performance of short codes are well studied in the literature and can be significantly enhanced by selecting an appropriate parity check matrix  $\mathbf{H}$  with Tanner Graph-based decoding as described in [10]. It is also possible to build more powerful codes by concatenating shorter codes which offer improved performance in terms of erasure recovery and result in better spectrum efficiency.

The rest of the article is structured as follows. The related work section is next. The system model and problem formulation is described in Section II. We describe the application of parity check equations on a packet level, and the recovery of missing packets using Tanner graph-based decoding in Section III. Section IV defines the metrics, which will be employed to fairly compare various erasure correcting codes applied in various channel occupancy and sensing conditions. Numerical simulation results are presented in Section V, highlighting comparisons between short erasure codes and long codes. Section VII concludes the paper by providing future direction of this work.

#### A. Related work

**LTE/WiFi coexistence:** Challenges of achieving harmonious coexistence of 5G NR-U and WiFi have been studied in the literature as detailed in [11]. There is abundant work including

analytical modelling, experimental results and system-level simulations. Analytical modelling and analysis of the coexistence of LTE in Unlicensed Spectrum and WiFi was addressed in [12]. Multi User Orthogonal Frequency Division Multiple Access (MU-OFDMA) transmissions were also considered for the coexistence in [13]. The work in [14] proposed a model to examine the coexistence of LTE and WiFi using a stochastic geometry approach. [15] proposed to mitigate interference for LTE-U that utilizes the ALOHA-like random access protocol and WiFi that is based on carrier sensing/energy detection prior to data transmission. The authors derived the spatial throughput and coverage probability for LTE-U & WiFi and performed asymptotic analysis for large numbers of the LTE-U nodes and WiFi. [16] investigated the impact of adjusting energy detection threshold on decoding capability of coexistence scenarios. Considering a game-theoretic approach, in [17] and [18], the authors showed that through fair spectrum sharing, better bit rate can be achieved in coexistence scenarios.

**Hidden node problem in WiFi:** The concept of hidden node problem has been well studied in the context of overlapping WiFi Access Points (WiFi/WiFi coexistence) and is commonly addressed by the feedback from the access nodes via request-to-send/clear-to-send (RTS/CTS) packets, which are received by all radio transceivers in range, at the cost of additional delay. However, like in LAA, NR-U can not use the RTS/CTS in WiFi/5G coexistence because they cannot decode each other's packets. Furthermore, the asymmetry of LAA and WiFi energy detection levels may cause the WiFi user's RTS packets to be ignored by the AP.

**Hidden node problem in LAA/5G NR-U:** Apart from a few recent studies, the analysis of hidden node problem in the context of LAA is really scarce. In [19], the hidden-node problem is addressed, in 20 MHz, by ns-3 simulations. The Channel Quality Indicator (CQI), Reference Signal Received Power (RSRP), and Reference Signal Received Quality (RSRQ) metrics at the LAA client device are used to develop a collision detection algorithm that is then used to modify the LAA MAC parameters. Other papers used duty cycle method instead of LBT [20]. In [21] a hybrid adaptive channel access scheme, which performs a flexible handoff between duty cycle muting (DCM) and LBT mechanisms is proposed to facilitate coexistence between LTE-U and legacy WiFi networks. This study is followed by the Cournot game approach in the duty cycle in CSAT Algorithm [22]. Authors in [23] studied the feasibility of supervised machine learning approaches in identifying UE in LAA networks that are being affected by collisions from hidden nodes sources and concluded that machine learning approaches are not necessarily better than heuristic-based solutions. In [24], [25] the authors studied LAA/WiFi coexistence real-world deployment and concluded that WiFi devices data rate can drop by up to 97%, while LAA users can see 35% of throughput fade.

**Long codes:** Channel coding is primarily used to correct errors as a result of weak signals. However, the technique can not distinguish if the error is caused by collision, interference or random noise. Therefore, correction techniques attempt to recover all errors equally. Recovering lost data as a result of imperfect sensing was addressed in [26], [27] and [28] by

means of erasure correcting codes, using LT-codes or Raptor codes, respectively. These long fountain codes were specifically designed to address broadcast multimedia applications, where decoding of large amounts of data is required. Rateless codes operate on hundreds of packets and are not suitable for low-latency communications.

**Short codes:** Short codes such as Single Parity Check Product Codes (SPCPCs) were studied in [29] as an instance concatenated codes, initially introduced for a binary erasure channel. The main interest of concatenating Single Parity Check (SPC) codes is achieving decoding simplicity, particularly in iterative decoding cases. SPCPCs had also been proposed for erasure recovery in the context of Asynchronous Transfer Mode (ATM) cells lost in congestion [30]. Short codes were not investigated in the context of 5G/WiFi coexistence for correcting erasure packets. To tackle errors resulting from collisions due to coexistence, we investigate the use of several short block codes, emphasising their advantages compared to various 5G/WiFi standardised methods.

**Current cellular standards:** Release 15 of the 3rd Generation Partnership Project (3GPP) 5G NR introduced two channel coding schemes: LDPC and Polar codes [31] at the physical layer to substitute the Turbo and convolutional codes applied in the 4G/LTE standards. In 5G, capacity-achieving LDPC codes are deployed in the user/data plane to support high throughput and error correcting capability with variable code rate, code length and compatibility with automatic repeat requests. On the other hand, Polar codes are adopted in the control plane, providing high performance with large block lengths [32]. For example, Polar codes are now the standard coding for eMBB (Enhanced Mobile Broadband) control channels for the 5G NR (New Radio) interface. The design of the Polar codes allows us to achieve capacity with asymptotically large block sizes, using successive cancellation decoding approaches. However, with the small block sizes, preferred by the industry, the performance of the successive cancellation is weak compared to schemes such as LDPC and turbo code. Successive cancellation list decoding offers improved efficiency, but its practicality is limited due to its iterative decoding nature. Several proposals were recently presented in the literature to tackle the issue. And [33], [34] and [35] shown promising performances under list decoding with small list size. The focus of this paper however is beamed towards low latency, user plane communications, using short length block codes with lower decoding complexity.

Polar codes, built on the concept of channel polarization, with list decoding structure and with infinite or finite code lengths, are fundamentally different from LDPC and short-block codes. For example, we used Tanner graph-based decoding on short and long block codes to compare the performance of our proposed Product and concatenated codes with LDPC, using various  $H$  matrices, but we cannot directly compare their performances with Polar codes using the same approach.

Carefully studying the suitability of Polar codes in coexistence settings, requires special mathematical (or statistical) treatments as well as complex decoding algorithms. We leave these additional challenges as future work.

**WiFi standards:** The WiFi bands are divided into non-

overlapping channels of 20 MHz bandwidth, which can be bonded to form wider channels. For example, IEEE 802.11ax has different channel configurations options ranging from 20-160MHz in both the 2.4GHz and 5GHz spectrum. 802.11ax standard (latest release) recommends to use LDPC codes when operating on large bandwidths (i.e., 80MHz & 160MHz) and to use Binary Convolutional Coding (stream-based) in narrower bandwidths (i.e., 20MHz, 40MHz & 60MHz). However, due to the nature of the channel layout and lack of available spectrum, larger bandwidths such 160MHz are rarely used in dense deployments, in the 2.4 and 5GHz bands. Therefore, from a practical standpoint, only channels up to 80MHz are used in WiFi. In fact, the majority of WiFi deployments today are 40 MHz and 80 MHz, particularly in 5GHz band, and recent studies show that all current LAA deployments in a study in Chicago (USA) aggregate three 20 MHz unlicensed channels (60 MHz), thus potentially creating increased interference and collisions to WiFi operations. We propose the use of short block codes to recover the erasure resulting from the increased collisions. Because we are proposing short, product and concatenated codes, they can easily be implemented on smaller bandwidths, e.g. 20MHz, 40MHz and 60MHz. We can also apply them on larger bandwidths (80MHz) by means of applying concatenated and product schemes.

## B. Main contribution

The main contributions of this paper are summarized as follows.

- To the best of our knowledge, we are the first to consider the use of short erasure block codes to optimize latency in the context of 5G/WiFi coexistence. In contrast to our work, only long and fountain stream-based codes were previously studied while current 802.11 standards and LTE/5G specifications recommend the use of convolutional and LDPC codes in data communications.
- We construct more sophisticated codes with less decoding complexity by utilizing concatenated (HammingSPC (1550, 1274)) and Product (Product Hamming(961, 676)) code schemes and show through experimental results the improved the spectral efficiency.
- We also develop an analytical model and derive the maximum achievable efficiency and Gaussian approximation efficiency estimation metrics, which take into account real-world constraints such as sensing parameters, code rate and failure probability to fully understand the impact of erasure codes in 5G/WiFi coexisting scenarios. Simulation vs. analytical comparisons with probability of false alarm confirmed the correctness of our efficiency estimates.
- We conduct a comprehensive evaluation to find the most suitable erasure codes for 5G/WiFi coexistence, considering various code lengths and number of samples, which corresponds to sensing time. We also provide detailed comparisons in respect of spectrum utilization, global throughput and failure probability of codes under varied number of coexisting users. Our comparisons include product and concatenated codes and leverage David J.C.

MacKay's data bases of sparse graph codes to obtain the parity check matrices, enabling decoding of signals.

## II. SYSTEM MODEL AND PROBLEM FORMULATION

In this section, we consider the coexistence of 5G NR-U and WiFi, two functionally different access technologies. We also describe our cross-layer design approach, combining CSMA/CA at the MAC layer with spectrum sensing at the physical layer. 5G NR-U may benefit from the contention based model, LBT, in its coexistence with WiFi using the same IEEE 802.11 mechanism to comply with spectrum regulations. Under LBT protocols, the channel availability is calculated via spectrum sensing at the physical layer and afterwards the packet transmission is controlled through the MAC layer protocol.

We propose a model of local networks for the coexistence of NR-U and WiFi, and assume that there are  $N$  WiFi stations (STA) connected through WiFi access point and 5G user equipment (UE) linked to gNodeB (gNB) of the NR-U. We refer to each user as an active user while it is transmitting data, and having an access to the channel after spectrum sensing as a result of applying the LBT protocol at layer 2 (MAC layer). Each UE shares the identical unlicensed spectrum with WiFi stations in a local network. The same energy detection is used by NR-U and WiFi at the PHY layer.

We also assume that each user has a continuous stream of data packets to transmit with non-empty transmission queue [36]. While typical WiFi networks are modelled with unsaturated traffic, in coexistence scenarios involving WiFi and 4G/5G, the common assumption is to analyze the performance under full load (at least 1 packet is waiting to be sent) [37], [38], [39], [40]. This assumption is important to provide worse case analysis to account for channel state during the backoff countdown process, resulting in a highly accurate estimation of collision probability, channel throughput and channel access delay. Changing this traffic pattern results in less collisions.

As cellular technologies fundamentally use scheduling-based channel access approaches, we assume such scheduler always enforces the usage of WiFi spectrum in situations where the 5G licensed bands are congested, and this is followed by using the contention-based distributed coordination function (DCF), the channel access MAC technique for IEEE 802.11-based standards. The DCF exploits the CSMA/CA with exponential backoff as shown in Fig. 1. To enable harmonious coexistence, we assume that NR-U devices follow a similar channel access process for coexistence with WiFi network [41].

A user equipment and a station initially sense the channel idleness before it transmits the data packets after using the distributed inter-frame space (DIFS) protocol. If the channel is busy, the station awaits for a randomly generated backoff period within the contention window (CW). The backoff has a range between 0 and  $\omega-1$  where  $\omega$  is the size of contention window. To minimise the implications of occupying the medium for too long (generating delays), we have used DCF mechanism and reduced the backoff contention window (CW) time (from  $60\mu$  to  $32\mu$  seconds) to retain equal access to

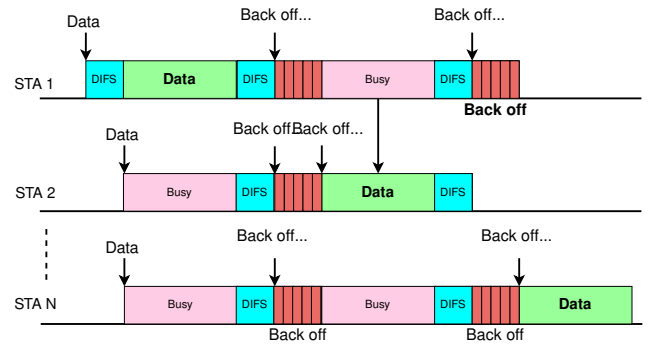


Fig. 1. Coexistence of 5G NR-U and WiFi using LBT

the channel and to avoid long channel occupancy by a single 5G UE. The slot for the contention window is initialized to minimum  $CW_{\min}$  for the first attempt [42]. Then, the backoff counter decrements the value until the channel becomes idle. The UE and the station then have access to the channel to start transmission again once the counter decrements to zero.

There is a negligible chance that two stations get a similar value of the backoff and start simultaneous transmission that will then result in a collision and lost data. However, energy detection, one of the most used spectrum sensing techniques at the PHY layer, suffers from inherent sensing impairments and does not distinguish between signal and noise, leading to detection errors. We mainly focus on the data lost due to sensing impairments that are potentially recoverable through the use of erasure-correcting codes.

The stations of WiFi or the UE of NR-U use the same access mechanism at the MAC layer as described earlier in this section. They have equal access to the bandwidth (without priorities or privileges), where the channel activity can be modelled as the succession of active and inactive intervals as described in [43]. As illustrated in Fig. 2, this process can be described by a two-state Gilbert model having transition probabilities from state *On* (active transmission) and state *Off* (idle). In this model, we assume that the given frequency band (channel) is organized into  $v$  equal width, multiple mutually exclusive subbands denoted as  $B_1, B_2, \dots, B_v$ , following the latest WiFi standard (802.11ax), which deploys orthogonal frequency-division multiple access (OFDMA), in the downlink and uplink. Each subband is either occupied (active transmission) or idle during each time slot  $\Delta T$ . In WiFi, some channels can be bonded to form wider channels. For example, IEEE 802.11ax has different channel configurations ranging from 20-160MHz in both the 2.4GHz and 5GHz spectrum. 802.11ax proposes to use LDPC codes when using large bandwidth (i.e., 80MHz & 160MHz) and to use Binary Convolutional Coding in narrower bandwidths (i.e., 20MHz & 40MHz) [44].

We refer to  $p_1$  and  $p_2$  to denote the transition probabilities from state *On* to state *Off* and vice-versa, respectively [45]. The steady state probabilities of *On* and *Off* states, respectively, are given by

$$P_{on} = \frac{p_2}{p_1 + p_2} \quad \text{and} \quad P_{off} = \frac{p_1}{p_1 + p_2}.$$

The activity of each user is uncontrollable as it is varying, which poses challenges to maintain and guarantee the

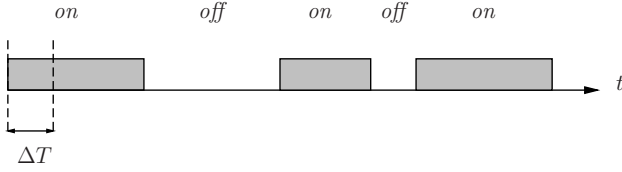


Fig. 2. The user activity representation in time domain.

quality of service (QoS). Through sensing activity, the users continuously observe the channel to identify the idle slots. A portion of the time-slot  $T_s$  is therefore dedicated for channel sensing, while the rest of the interval  $T - T_s$  is utilized for the transmission of active user if no other transmission is present.

The sensing impairments, captured by false alarm  $P_{FA}$  and non-detection  $P_{ND}$  probabilities, are inter-dependent. This interdependence can be described using the Receiver Operating Characteristic Curve (ROC) [46]. The challenge herein is that it seems unlikely to simultaneously maintain small values for both probabilities. Instead, it is necessary to identify a feasible operating point on the ROC graph.

Although protection of data packets happens at the physical layer by error correcting codes, several packets could still be lost because of interference and collisions. The lost data can be considered as erased. To retrieve the missing data, an erasure correcting code  $\mathcal{C}(n, k)$  can be added to operate at the application layer. To reduce the impact of collisions on network latency and spectrum efficiency, we propose the use of short block codes, and construct new concatenated codes (HammingSPC) and products of short block codes such as Product Hamming and compare their performances against LDPC codes.

The code can be described using a set of parity check equations. This can be visualized using Tanner graphs and the equations are encapsulated in the rows of the parity check matrix. These parity check equations can be generalized to a packet level if data encoding occurs as packets  $P_1, P_2, P_3, \dots, P_n$ . In this case, all bits that compose a packet represent a codeword within the code set  $\mathcal{C}$ , as depicted in Fig. 3.

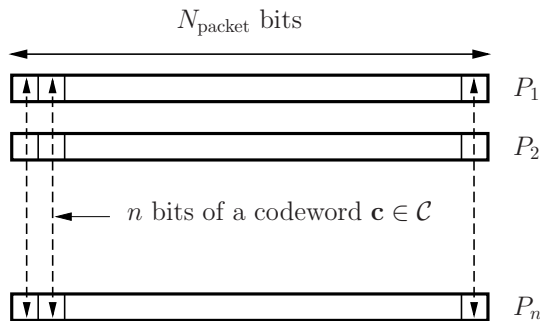


Fig. 3. Packet level coding

We denote the parity check matrix of the code  $\mathcal{C}$  as  $\mathbf{H}$ . The parity check equation can be represented as  $\sum_{j=1}^n h_{i,j} P_j = \mathbf{0}$ . For a single missing packet captured in this equation, recovery can be made by employing XOR operation to all the other packets. This process is illustrated in Fig. 4. This procedure is

invoked iteratively until no more erasure or until the equation with only a single erased packet cannot be found. The code performance can be calculated by a two-variable polynomial enumerator, as defined in [47]. This estimation attempts to enumerate all erasure patterns that are less likely recoverable post decoding. These non-recoverable instances are captured by the dead-end sets, defined as  $T(x, z) = \sum_{i,j=0}^n T_{i,j} z^j x^i$ , where  $T_{i,j}$  are total non-recoverable erasure patterns with initial size  $i$  and final size  $j$ . From this polynomial, we derive the following approximations:

$$p_r \approx \frac{1}{n} \sum_{i \geq 0} \left( \sum_{j > 0} j T_{i,j} \right) p^i (1-p)^{n-i} \quad (1a)$$

$$p_f \approx \sum_{i=0}^n T_i p^i (1-p)^{n-i}, \text{ with } T_i = \sum_{j>0} T_{i,j} \quad (1b)$$

In the above equation, we used  $p_f$  as the probability of having a non-complete recovery of all the erasures (failure probability), and  $p_r$  as the post-decoding residual erasure probability. These probabilities can capture the performance of erasure-correcting codes.

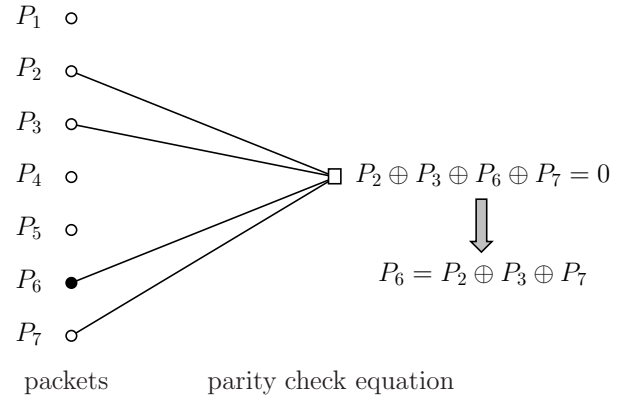


Fig. 4. Erased packet  $P_6$  can be recovered from a parity check equation

The probabilities  $p_f$  and  $p_r$  were computed under the assumption of a uniform distribution of independent erasures with a given collision probability,  $p$ , as in [48]. We further assume that the information packets  $(I_1, I_2, \dots, I_k)$  are encoded using a systematic erasure correcting code so that the information is apparent in each codeword, i.e.,

$$(I_1, I_2, \dots, I_k, R_1, R_2, \dots, R_{n-k})$$

where  $R_1, \dots, R_{n-k}$  constitute the redundant packets. For any systematic codes, the generator matrix  $\mathbf{G}$  of size  $k \times n$  can be written as

$$\mathbf{G} = (\mathbf{I}_k \mid \mathbf{A}) \quad (2)$$

where  $\mathbf{I}_k$  denotes the  $k \times k$  identity matrix, and  $\mathbf{A}$  is an arbitrary  $k \times (n - k)$  binary matrix. The code given by such a generating matrix has dimension  $k$ . Parity check matrix of size  $(n - k) \times n$  can be written as

$$\mathbf{H} = (\mathbf{A}^T \mid \mathbf{I}_{n-k}) \quad (3)$$

where  $\mathbf{A}^T$  is  $(n - k) \times k$  depicts the transpose matrix of  $\mathbf{A}$ , and  $\mathbf{I}_{n-k}$  is the  $(n - k) \times (n - k)$  identity matrix.

### III. SHORT BINARY ERASURE CORRECTING CODES

We provide some preliminaries regarding the binary erasure channel (BEC) and codes. Any binary linear code  $\mathcal{C}(n, k, d)$  of length  $n$ , dimension  $k$ , and minimum distance  $d$  has a basic property that these parameters are not independent. The Singleton bound (aka Joshibound) states that  $d \leq n - k + 1$ , which can be rewritten as  $d = n - (k + i) + 1$  for any  $i \geq 0$ . For the case of  $i = 0$ , we refer to these codes as Maximum Distance Separable (MDS) codes. The erasure correcting capability is given by  $n - (k + i) = d - 1$ . A very simple decoding algorithm can be constructed using the graphical representation of parity check equations of the code, namely Tanner graph. This decoding can be briefly described as follows.

We keep a record of erased positions at each iteration of the algorithm as a vector  $\mathbf{E}$ :

$$\mathbf{E}(i) = \begin{cases} 1 & \text{if position } i \text{ is erased} \\ 0 & \text{otherwise} \end{cases}$$

With this vector, we can easily compute the *index* of a parity check equation defined as the number of erased positions in this equation. All these indexes can be stored in a vector

$$\mathbf{Index} = (\mathcal{I}_1, \mathcal{I}_2, \dots, \mathcal{I}_{n-k}) = \mathbf{H} \cdot \mathbf{E}^t,$$

where the representation follows the traditional arithmetic operations of natural numbers. We can distinguish some particular cases depending on the values of the integer components of this index vector as follows.

- When  $\mathcal{I}_j = 0$  then we consider that there is no erased position in parity check equation  $j$ .
- For  $\mathcal{I}_j = 1$ , we have a single erased position in parity check equation  $j$ . In this instance, we can recover the erased position by XORing other non-erased packets involved in that equation.
- For  $\mathcal{I}_j > 1$ , we have two or more erased positions in parity check equation  $j$ . This instance indicates that erasures might not be recoverable.
- When  $\mathbf{Index} \neq \mathbf{0}$  contains no parity check equation with a single erased position, it means recovery can not go further and fails. Such erasure patterns are called stopping sets.

The iterative recovery consists of, at each iteration, searching for a parity check equation with index one; if we find one we recover the erased position involved in this equation and update the vector recording erasures (and decrement the corresponding index values). This is a greedy algorithm, which does not involve complicated operations (only XOR operations). The algorithm ends when there is no more erasure or no equation with index 1.

Furthermore, Schwartz and Vardy [10] have shown that incorporating redundant parity check equations to  $\mathbf{H}$ , called extended parity check matrix  $\mathbf{H}_e$ , enables the recovery of erasure patterns up to  $d - 1$  for strongly structured codes such as Golay and Reed-Muller. There is also a possibility of using cyclic codes BCH to achieve an extended  $\mathbf{H}_e$  matrix with this approach. These additional parity check equations are obtained by applying the cyclic shift using the basis vector at

the expense of a slightly higher decoding time, but significant improvement will be observed in the erasure recovery, which will result in higher achievable efficiency for spectrum reuse. We will also use the product and concatenated codes to obtain erasure recovery and their decoding procedure as described in the following subsection.

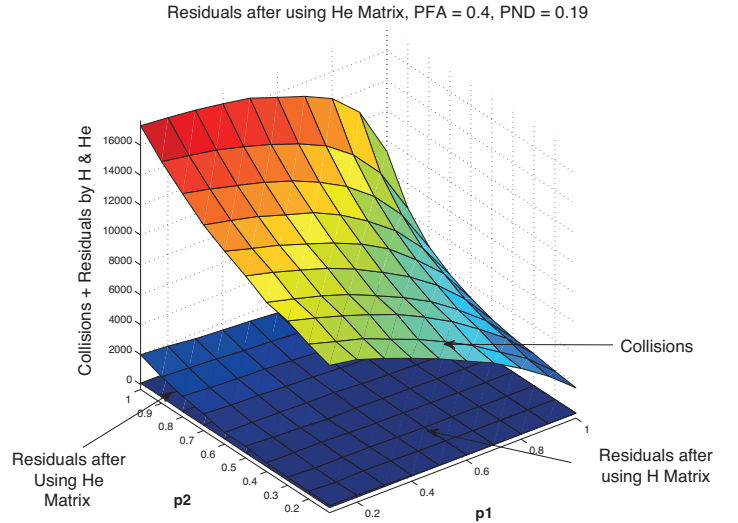


Fig. 5. Collisions and Residuals after block codes

Furthermore, we have plotted 3D curves as shown in Fig. 5 to show the distribution of collisions before decoding and residuals (the remaining errors which cannot be decoded correctly) after decoding using block codes. The top curve shows the collisions when no erasure codes are used. When we use the erasure correcting codes with  $\mathbf{H}$  matrix we can recover multiple erasures accrued due to collisions as shown in the middle curve. The middle curve shows that we have recovered maximum collisions and few residuals are remaining which can be further reduced when using  $\mathbf{H}_e$  matrix. The bottom curve shows the residuals when using the  $\mathbf{H}_e$  matrix of the codes that now contain very limited collisions. We can easily observe very few residuals are there when using  $\mathbf{H}_e$  matrix as it will improve the code performance. Our results include the use of enhanced parity check matrix.

#### A. Single Parity Check Product and Concatenated Codes

Single Parity Check SPC codes  $(k + 1, k, d = 2)$  have been applied for error detection and single erasure correction [49]. The codes contain  $k$  information packets  $(I_1, \dots, I_k)$  extended with a parity packet  $I_{k+1} = I_1 \oplus I_2 \oplus \dots \oplus I_k$  to constitute a codeword. Erasures can be detected and recovered by applying the serial concatenation for two SPC codes, namely  $\text{SPC}(k_1 + 1, k_1, 2) \times \text{SPC}(k_2 + 1, k_2, 2)$ . Such operation forms the product code that represent a rectangular array where the rows utilize a  $(n_1, k_1, d_1)$  code and the columns use a different  $(n_2, k_2, d_2)$  code. The overall length, dimension and minimum distance of this resulting code are given by  $n = n_1 \times n_2$ ,  $k = k_1 \times k_2$ , and  $d = d_1 \times d_2$ , respectively. The block diagram of this  $(n_1 \times n_2, k_1 \times k_2, d_1 \times d_2)$  product code is shown in Fig. 6.

The erasure recovery is relatively straightforward as it only involves XORing packets around a given parity check

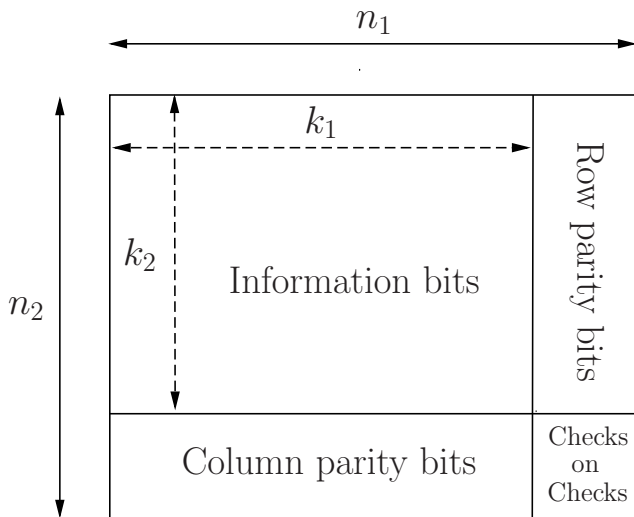


Fig. 6. Two dimensional product codes matrix. For SPCPC we have  $n_1 = k_1 + 1$  and  $n_2 = k_2 + 1$

equation. For an SPC, we can carry out a single erasure recovery by applying this XORing within the equation  $I_1 \oplus I_2 \oplus \dots \oplus I_k \oplus I_{k+1} = 0$ , where  $I_1 \dots I_k$  corresponds to  $k$  information packets and  $I_{k+1}$  is the parity check packet that composes a codeword. As an illustration, if packet  $I_e$  becomes the sole erased packet, the recovery can be made using

$$I_e = \sum_{j \neq e} I_j. \quad (4)$$

If there are two or more erased positions in a row or a column, then erasure recovery is not possible but we can apply an iterative procedure which is described next for an SPCPC( $n_1 \times n_2, k_1 \times k_2, d_1 \times d_2$ ) product code.

We first perform row erasure decoding on all rows. After row decoding, some erasures will remain as mentioned above, but the total number of erasures should have decreased. We then perform the same technique on the columns, achieving a lower number of erasures after this step. The similar iterations on row and column decoding are continued up to the point of no residual erasure or non-recoverable erasures. To enhance the erasure recovery capability, the decoding for product of short codes Hamming  $\times$  Hamming( $15 \times 15, 11 \times 11, 3 \times 3$ ) can be performed at the expense of reduced code rate to half. In order to enhance the code rate, there is a possibility to concatenate short block codes with SPC by decoding short block codes for rows and a single parity check for columns (e.g., Hamming  $\times$  SPC ( $15 \times 6, 11 \times 5, 3 \times 2$ ). The performance of LDPC codes will be compared with the performance of short block codes and product codes as described above with the simulation results presented in Section V.

#### IV. PERFORMANCE ANALYSIS

##### A. Efficiency metrics

We need to establish a criterion to carry out a fair comparison for erasure correction capability across a variety of short codes, including BCH, Hamming, Golay, and long codes, e.g., LDPC. The spectral efficiency depends on three chief

parameters; code rate; the WiFi STAs and 5G UE activity; and sensing impairments. The code rate defines the total number of useful information packets received by the WiFi STAs and 5G UE, where block codes with a higher rate produce an improved spectral efficiency. The code rate  $k/n$  also indicates the amount of redundancy introduced to the information packets for erasure recovery of erased data packets. On the other hand, increasing the value of  $on$  probability  $P_{on}$  reduces the time available for other users for data transmission, which inevitably impacts efficiency. Sensing impairments could further impact the operation through false alarm probability  $P_{FA}$ , generating missed access to the channel and reduced number of packet transmissions. Additionally, non-detection probability  $P_{ND}$  may also add collisions to the operation of WiFi STAs and 5G UE and this will ultimately compromise the ability to recover erasures.

In the two extreme conditions,  $P_{FA} = 0$  corresponds to a case of persistent channel access at the expense of high collision probability with an already active user, while  $P_{FA} = 1$  refers to a situation of persistent collision avoidance, which implies zero efficiency due to the lack of channel access. Note that there is a direct link between erasure recovery and efficiency. Another important parameter which impacts efficiency is the minimum distance  $d$  of the code since it indicates the erasure correction capability of up to  $d - 1$ , correcting all erasure patterns of at most  $d - 1$  erasure(s).

Appropriate selection of the parity check matrix is critical for the erasure correction capability. A potential direction is to use cyclic codes along with an extended parity check matrix  $\mathbf{H}_e$ . A criterion can be defined to showcase the effects of this parameter selection. We first state an at detector reference, i.e.,  $P_{FA} = 0$  and  $P_{ND} = 0$ , which implies the ability of all users to utilize all idle times. Suppose that for  $t \gg 1$  consecutive time-slots, we have  $t \times P_{off}$  slots are free, on average. We can calculate the average number of packets correctly transmitted by the active users (WiFi STAs and 5G UE) as

$$N_p(\text{ideal}) = t \times P_{off}. \quad (5)$$

Equation (5) governs the idealistic scenario by the active user with the ideal detector since redundant packets are not required (no collision) and all opportunities are utilized. However, in a realistic condition, we need to consider the impact of sensing impairments. In this case, the average number of transmitted packets of the active user becomes

$$N_p(\text{real}) = t \times \left( P_{on} P_{ND} + P_{off} (1 - P_{FA}) \right). \quad (6)$$

Collisions result in erased packets for the active user. We can express the collision probability  $p$  conditioned on any other user's transmission as

$$p = \frac{P_{on} P_{ND}}{P_{on} P_{ND} + P_{off} (1 - P_{FA})}. \quad (7)$$

The average number of codewords that are transmitted by an active user is then equal to  $N_p(\text{real})/n$ , and  $(1 - p_f)$  is a fraction of codewords that are recovered completely after decoding. The code rate is an important parameter here that contains  $k$  information packets and  $n$  transmitted packets. In

this way, the average received  $k$  information packets over  $t \gg 1$  becomes

$$N_p(\text{info}) = k \times \frac{N_p(\text{real})}{n} \times (1 - p_f). \quad (8)$$

Now, we can represent the efficiency as

$$\eta_c = \frac{N_p(\text{info})}{N_p(\text{ideal})}. \quad (9)$$

Next, we substitute (8) and (5) in (9) to obtain

$$\eta_c = \frac{k}{n} \times \frac{1}{P_{\text{off}}} \left( P_{\text{on}} P_{\text{ND}} + P_{\text{off}} \times (1 - P_{\text{FA}}) \right) \times (1 - p_f). \quad (10)$$

The comparison of efficiency  $\eta_c$  for multiple block codes with different code rates is fair: As the different block codes can be compared for the same value of  $P_{\text{on}}$  (with the same idle slots available) and the efficiency  $\eta_c$  is directly proportional to throughput. By using the efficiency expression provided above, we can also derive the efficiency parameter without using channel coding, which is represented as uncoded efficiency  $\eta_u$ . Encoding becomes equivalent to rate one code with  $n = k$ , which implies that the probability of correctly receiving information packets by the active user without collision becomes  $(1 - p)^k$ . We then multiply the probability  $(1 - p)^k$  expression instead of  $(1 - p_f)$  with the efficiency  $\eta_c$ . After simplification, we get the efficiency formula without coding and

$$\eta_u = \frac{N_p(\text{info})}{N_p(\text{ideal})}$$

becomes

$$\eta_u = \frac{P_{\text{off}}^{k-1} (1 - P_{\text{FA}})^k}{\left( P_{\text{on}} P_{\text{ND}} + P_{\text{off}} \times (1 - P_{\text{FA}}) \right)^{k-1}} \quad (11)$$

We have plotted the efficiency curves with and without erasure coding to analyse the differences. We have plotted the efficiency curves using equation (11) for  $k = 12$  and  $k = 21$  as shown in Fig. 7. We can see the difference in the efficiencies when plotting with erasure correcting codes BCH(31,21) and Golay(24,12) using equation (10). The efficiency achieved using Golay(24,12) code is 43% which is significantly higher than the efficiency achieved using BCH(31,21) which is 37%.

### B. Analytical Approximation for Efficiency

Our simulation results show that the efficiency  $\eta_c$  as a function of false alarm probability  $P_{\text{FA}}$  is upper bounded by a simple function of  $1 - P_{\text{FA}}$ , as the active user's occupancy probability  $P_{\text{on}}$  remains low. In order to derive this property, we proceed through existing computations for the false alarm and non-detection probabilities.

We assume that there are a number of samples  $\{X_1, X_2, \dots, X_n\}$  corresponding to two hypotheses  $H_0$  (with no signal containing only noise) or  $H_1$  (when the signal is present with noise). Quantity  $Y$  is computed from these samples, for instance  $Y = \frac{1}{n} \sum_{i=1}^n X_i^2$  for energy detection, but any function  $Y = f(X_1, X_2, \dots, X_n)$  could be provided to compute the conditional distributions  $\Pr[y|H_0]$  and  $\Pr[y|H_1]$ .

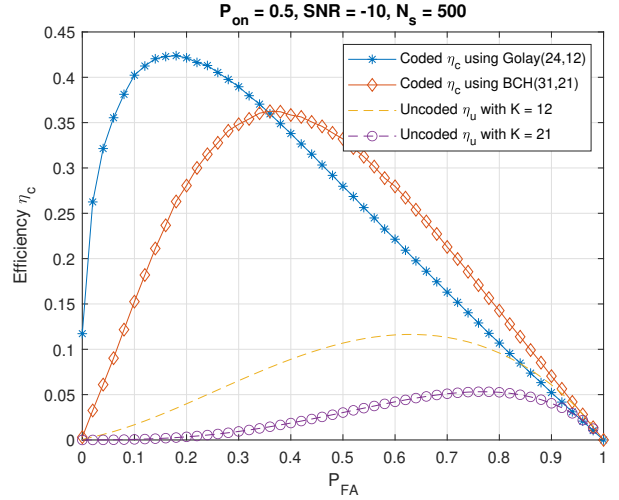


Fig. 7. Comparison of Efficiency with and without Erasure Coding

We then use this property that generally the two distributions are significantly different<sup>1</sup>:  $\Pr[y|H_0]$  is rather located for the small values (that means there is no signal contributing to  $y$ ) while  $\Pr[y|H_1]$  is rather located near the greater values of  $y$ .

We use a threshold  $\gamma$  and decide when  $y > \gamma$ , the hypothesis  $H_1$  is true, and conversely, when  $y < \gamma$  the hypothesis  $H_0$  is true.

### C. The Gaussian approximation

When the number of samples  $n$  in  $Y = \frac{1}{n} \sum_{i=1}^n X_i^2$  is sufficiently large, the central limit theorem [50] implies that the behaviour of  $Y$  can be approximated as a Gaussian random variable with the associated mean and variance as

$$m_Y = \frac{1}{n} \sum_{i=1}^n \mathbb{E}[X_i^2] = \sigma_X^2 \quad (12)$$

$$\sigma_Y^2 = \mathbb{E}[Y^2] - \mathbb{E}[Y]^2 = \frac{2}{n} \sigma_X^4, \quad (13)$$

respectively. The practical choice of  $n$  depends on  $P_{\text{FA}}$  and the operating SNR range with an accurate energy detection typically obtained with  $n$  in the order of  $10^1 - 10^2$  [51]. Larger  $n$  implies larger latency in making the decision of signal presence.

The two possible hypotheses  $H_0, H_1$  are defined by a different power of  $X_i$ . In no-signal hypothesis ( $H_0$ ), we have  $\sigma_X^2 = \sigma^2$  (that is the noise variance) and  $Y$  is a normal variable  $(m_Y, \sigma_Y)$  with

$$\begin{cases} m_Y = \sigma^2 \\ \sigma_Y^2 = \frac{2}{n} \sigma^4 \end{cases}$$

Given the threshold  $\gamma$  it is possible to compute the false alarm probability as

$$P_{\text{FA}} = Q\left(\sqrt{\frac{n}{2}} \times \frac{\gamma - \sigma^2}{\sigma^2}\right),$$

<sup>1</sup>if not then it means the quantity  $Y$  we are using is not a good variable for the detection

where  $Q(x)$  is the standard tail probability function that is defined by

$$Q(x) = \frac{1}{\sqrt{2\pi}} \int_x^{\infty} e^{-t^2/2} dt.$$

When the signal with power  $P$  is present ( $H_1$ ), we have  $\sigma_X^2 = P + \sigma^2$  and the mean and variance of  $Y$  can be written as

$$\begin{cases} m_Y = \sigma^2 + P \\ \sigma_Y^2 = \frac{2}{n} (\sigma^2 + P)^2 \end{cases}$$

We now calculate the non-detection probability  $P_{ND}$  as

$$P_{ND} = 1 - Q\left(\sqrt{\frac{n}{2}} \times \frac{\gamma - (\sigma^2 + P)}{\sigma^2 + P}\right).$$

We make use of the property  $Q(-x) = 1 - Q(x)$ ,  $\forall x \in \mathbb{R}$  to write

$$1 - P_{FA} = Q\left(\sqrt{\frac{n}{2}} \times \frac{\sigma^2 - \gamma}{\sigma^2}\right) \quad (14a)$$

$$P_{ND} = Q\left(\sqrt{\frac{n}{2}} \times \frac{\sigma^2 + P - \gamma}{\sigma^2 + P}\right). \quad (14b)$$

The case where the false alarm probability approaches 1 ( $P_{FA} \rightarrow 1$ ), it means that  $m_Y - \gamma \gg \sigma_Y$  or equivalent to

$$1 - \frac{\gamma}{\sigma^2} \gg \sqrt{\frac{2}{n}}. \quad (15)$$

Equation (15) indicates that  $\gamma$  is such that the arguments of the two Q-functions are much greater than 1, so that we can use the approximation

$$Q(x) \approx \frac{1}{x\sqrt{2\pi}} \times e^{-x^2/2}, \quad (16)$$

to obtain

$$1 - P_{FA} \approx \frac{1}{\sqrt{n\pi}} \frac{\sigma^2}{\sigma^2 - \gamma} \exp\left\{-\frac{n}{4} \left(\frac{\sigma^2 - \gamma}{\sigma^2}\right)^2\right\}, \quad (17a)$$

and

$$P_{ND} \approx \frac{1}{\sqrt{n\pi}} \frac{\sigma^2 + P}{\sigma^2 + P - \gamma} \exp\left\{-\frac{n}{4} \left(\frac{\sigma^2 + P - \gamma}{\sigma^2 + P}\right)^2\right\}. \quad (17b)$$

Now if we take the logarithm of both sides of (17a) and (17b) we get

$$\log\left[\sqrt{n\pi}(1 - P_{FA})\right] \approx -\frac{n}{4} \left(1 - \frac{\gamma}{\sigma^2}\right)^2 - \log\left(1 - \frac{\gamma}{\sigma^2}\right) \quad (18)$$

$$\begin{aligned} \log\left[\sqrt{n\pi}(P_{ND})\right] &\approx -\frac{n}{4} \left(1 - \frac{\gamma}{\sigma^2 + P}\right)^2 - \\ \log\left(1 - \frac{\gamma}{\sigma^2 + P}\right). & \end{aligned} \quad (19)$$

Lastly, we make use of the fact that  $\frac{\gamma}{\sigma^2} \ll 1$  to derive the first order approximations as follow:

$$\begin{aligned} \log\left[\sqrt{n\pi}(1 - P_{FA})\right] &\approx -\frac{n}{4} \left(1 - 2\frac{\gamma}{\sigma^2}\right) + \frac{\gamma}{\sigma^2} = \\ &-\frac{n}{4} + \frac{\gamma}{\sigma^2} \left(1 + \frac{n}{2}\right) \end{aligned} \quad (20)$$

And likewise, the approximations for  $P_{ND}$  is as follows:

$$\log\left[\sqrt{n\pi}P_{ND}\right] \approx -\frac{n}{4} + \frac{\gamma}{\sigma^2 + P} \left(1 + \frac{n}{2}\right) \quad (21)$$

We can eliminate  $\gamma$  between these two approximations to get an approximation of  $P_{ND}$  as a function of  $1 - P_{FA}$  as

$$\begin{aligned} \sqrt{n\pi}P_{ND} &\approx \left[\sqrt{n\pi}(1 - P_{FA})\right]^{\frac{1}{1+\text{SNR}}} \times \\ &\exp\left\{-\frac{n}{4} \times \frac{\text{SNR}}{1 + \text{SNR}}\right\} \end{aligned} \quad (22)$$

We first define the signal-to-noise-ratio (SNR) as:

$$\text{SNR} = P/\sigma^2.$$

Now we can substitute (22) in equation (10) to get the efficiency formula (23). And we can compare this analytical approximation with the simulated results across various codes, as shown in Fig. (8). We can observe that the simulation results closely match our analytical approximations.

#### D. Effect of sensing related parameters

The number of samples  $N_s$  has a significant effect on the efficiency, as expected, and it has been explained with the help of Fig. 9. It is clear that for the same target value of  $P_{ND}$ , the optimum probability of false alarm decreases with the increase of  $N_s$  and active users have more opportunities to access the channel.

Fig. 10 depicts the simulation results using Hamming(15,11) code. We analyze that the efficiency  $\eta_c$  achieves higher values as the number of samples  $N_s$  are increased for the same values of  $P_{FA}$ .

It is also noticed that when  $P_{FA} \approx 0$ , the transmitting user has full access to the channel all the time, with a very high collision probability to any other user waiting for transmission and the code (with a modest erasure correction capability such as Hamming(15,11) with  $d = 3$ ) cannot recover high erasures. As a result, WiFi STAs and 5G UE both have limited successful accesses to the channel (during coexistence operation). Similarly, when  $P_{FA} \approx 1$ , the efficiency is close to zero due to the fact that the active user has no access to the channel. The maximum efficiency is achieved as a result of two effects: (1) as  $P_{FA}$  increases, few opportunities are missed by the user, but the number of collisions (erasures) decreases, where the code is able to recover these erasures. (2) If  $P_{FA}$  is too high then the efficiency suffers mainly due to the reduced number of channel access instances and the efficiency ultimately decreases. This shows that the choice of a good functioning point ( $P_{FA}, 1 - P_{ND}$ ) on the ROC curve will have a significant impact on the performance of spectrum use.

#### E. Maximum Achievable Efficiency $\eta_{max}$ Estimation

Maximum achievable efficiency for spectrum use can be estimated using the following derivation: The maximum number of transmitted packets by the user in the channel is defined as

$$P_{trans} = t \times \left(P_{on} P_{ND} + P_{off} \times (1 - P_{FA})\right), \quad (24)$$

$$\eta_c \approx \frac{k}{n} \times \frac{1}{P_{off}} \left( \frac{P_{on} [\sqrt{n\pi} (1 - P_{FA})]^{\frac{1}{1+SNR}} \times \exp \left\{ -\frac{n}{4} \times \frac{SNR}{1+SNR} \right\}}{\sqrt{n\pi}} + (P_{off} \times (1 - P_{FA})) \right) \times (1 - p_f). \quad (23)$$

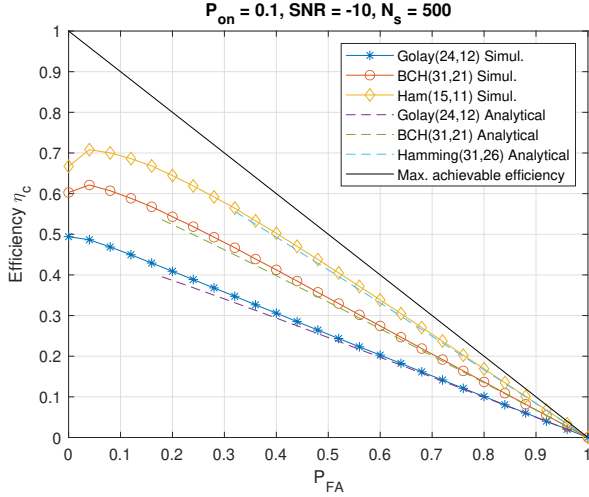


Fig. 8. Comparison of simulation vs. analytical approximation of efficiency  $\eta_c$

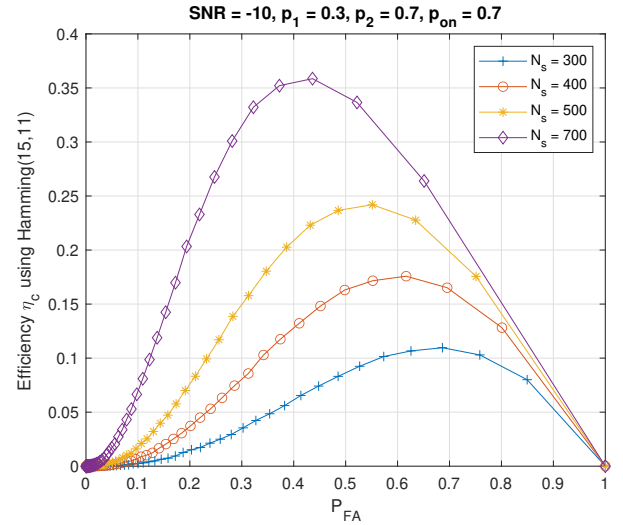


Fig. 10. Efficiency  $\eta_c$  with Hamming(15,11) code, for several values of  $N_s$

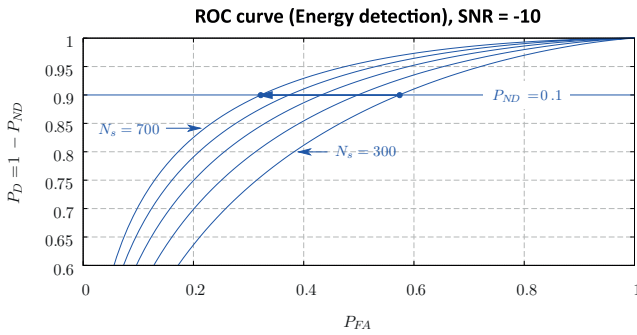


Fig. 9. Changing the number of samples:  $N_s = 300, 400, \dots, 700$

whereas the maximum number of correctly received packets by any receiver is given by

$$\eta_{max} = P_{trans} \times (1 - p). \quad (25)$$

Using equations (7), (10) and (25), the following expression for maximum achievable efficiency is obtained after simplification:

$$\eta_{max} = (1 - P_{FA}) \quad (26)$$

We will observe from the simulation results, in the next section, that the codes with strong erasure recovery capability achieve an  $\eta_c$  versus  $P_{FA}$  curve closer to the maximum achievable efficiency  $\eta_{max}$  which is indeed an upper bound for efficiency  $\eta_c$ . In the next section, various simulation results

are provided that will give a comparison to achieve various efficiency levels using short, long, product and concatenated erasure correcting codes.

## V. SIMULATION RESULTS

In order to analyze the effect of various parameters on efficiency (as defined in section IV) for the scenario defined in section II, we performed several simulations by varying the WiFi STAs and 5G UE transmission activity, sensing parameters and the parameters of block codes. To take into account the collisions introduced by the sensing scheme (energy detection and the difference in access parameters like transmission duration (TXOP)) we used ROC curve giving the detection probability  $P_D$  as a function of the false alarm probability  $P_{FA}$ . Given a value of  $P_{FA}$  it is easy to generate collisions (erasures) with a probability  $1 - P_D$  for each packet by moving on the ROC curve that corresponds to different values of  $P_{FA}$ . Encoding, decoding and simulations are all performed using integrated development environments (IDE) code blocks, written in C++. MATLAB and GnuPlot were used to plot the results. The parity check matrices of various LDPC codes to perform decoding are taken from David J.C. MacKay's databases of error-correcting codes<sup>2</sup>.

We have performed various simulations for a fixed  $P_{on}$  to evaluate the effect on efficiency, using various short and long codes with different lengths, minimum distances (providing erasure correction capabilities) and code rates. The procedure is repeated for different values of  $P_{on}$  probability.

<sup>2</sup>see : Encyclopedia of Sparse Graph Codes, available online at <http://www.inference.phy.cam.ac.uk/mackay/codes/data.html>

TABLE I  
THE EFFECT OF CODE LENGTH AND USER'S ACTIVITY  $P_{on} = 0.1$  ON  
EFFICIENCY  $\eta_c$

Setting Parameters:  $P_{on} = 0.1$ , SNR = -10 dB,  $N_s = 500$

Code	Rate	Optimal $P_{FA}$	$\% \eta_c$
Hamming(63,57)	0.89	0.1	70
LDPC(96,48)	0.5	0	55
LDPC(495,433)	0.88	0.05	83
LDPC(4376,4094)	0.94	0.15	80

#### A. Effect of code length and $P_{on}$ on efficiency $\eta_c$

It is assumed that the system allows a maximum 10% of collisions, implying that the input collision probability  $p$  with any other user should not be greater than 10%. The effect of code lengths on efficiency is compared for different classes of codes, including short block codes and LDPC codes. We observe from the simulation results that the transmission activity  $P_{on}$  has an effect on the WiFi STA and 5G UE efficiency. The best efficiency is achieved for small values of  $P_{on}$  when  $P_{FA} \simeq 0$  and decreases as  $P_{FA}$  increases. This is because the active users, in a coexisting scenario, consume all available slots of the spectrum without experiencing too many collisions.

Fig. 11 represents efficiency comparisons, achieved using short codes and longer LDPC codes when the users' activity is equal to 0.1. Both categories exhibit comparable performances because there are not excessive amount of collisions and the short block codes are able to recover erased data as well as longer ones, as shown in Table I, when  $P_{on} = 0.1$ , SNR = -10 dB,  $N_s = 500$ .

The efficiency  $\eta_c$  achieved using the codes with length  $N < 100$ , Cyclic Hamming(63,57) having extended parity check matrix  $\mathbf{H}_e$  is significantly higher compared to  $\eta_c$  achieved when using LDPC(96, 48) code, and is a result of a better code rate (0.9 compared to 0.5 for the LDPC). However, using very long codes for example with  $N > 1000$ , LDPC(4376,4094), the achieved  $\eta_c$  is closer to maximum achievable efficiency  $\eta_{max}$ . These long codes are not suitable for delay-sensitive applications due to their inherent high decoding complexity.

Increasing the transmission time and user activity (from WiFi stations or 5G UE) leads to excessive collisions and an intolerable amount of lost data. This will limit the efficiency  $\eta_c$  reaching an optimum level. The same comparison for a higher value  $P_{on} = 0.5$  is performed and it can be observed in Fig. 12 that the achieved  $\eta_c$  is not as high as with  $P_{on} = 0.1$ . The comparison of various codes is given in Table II where we compare the achieved  $\eta_c$  of block codes with smaller length, when  $P_{on} = 0.5$ , SNR = -10 dB,  $N_s = 500$ . We compared the  $\eta_c$  of Hamming(15,11) codes with  $\mathbf{H}_e$  that is comparable with LDPC(273,191) code. We observed that the Hamming(15,11) code is preferable for the erasure recovery as it has a shorter length as compared to LDPC(273,191) code. However, longer length LDPC(4095,3357) and LDPC(1057,813) achieve  $\eta_c$  much closer to the upper limit of efficiency, due to the fact that these codes with longer lengths have strong erasure recoverability.

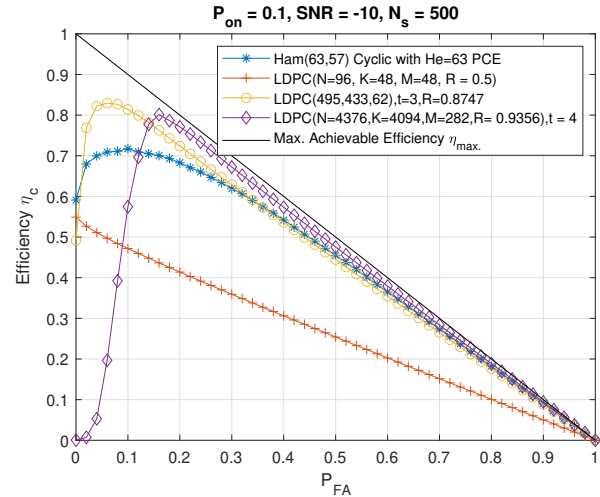


Fig. 11. Comparison of several codes,  $P_{on} = 0.1$ . Effect of code length on efficiency  $\eta_c$ . Three main cases :  $N < 100$ ,  $100 < N < 1000$ ,  $N > 1000$

TABLE II  
THE EFFECT OF CODE LENGTH AND USER'S ACTIVITY  $P_{on} = 0.5$  ON  
EFFICIENCY  $\eta_c$

Setting Parameters:  $P_{on} = 0.5$ , SNR = -10 dB,  $N_s = 500$

Code	Rate	Optimal $P_{FA}$	$\% \eta_c$
Hamming(15,11)	0.73	0.25	49
LDPC(273,191)	0.7	0.28	59
LDPC(1057,813)	0.77	0.38	55
LDPC(4095,3357)	0.82	0.52	45

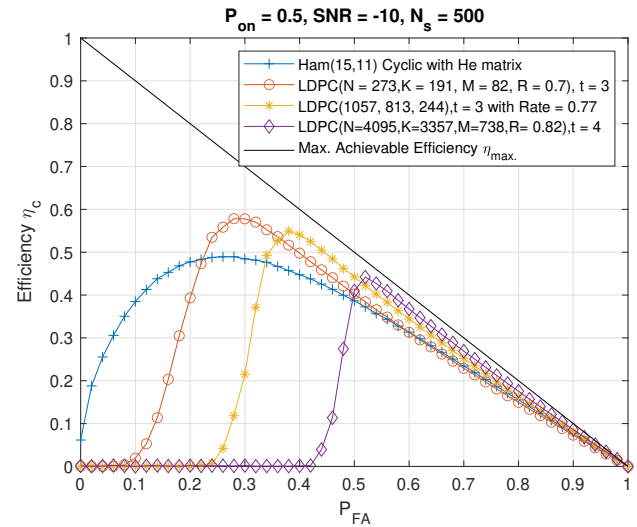


Fig. 12. Comparison of several codes,  $P_{on} = 0.5$ . Effect of code length on efficiency  $\eta_c$ . Three main cases :  $N < 100$ ,  $100 < N < 1000$ ,  $N > 1000$

#### B. Comparison of short block codes with short LDPC Codes

In this section, the simulations are carried out to define the performances of Hamming(63,57), Hamming(31,26), Hamming(15,11), BCH(31,21) and LDPC(96,48), providing a fair comparison of short block codes with short LDPC code. It is observed in the Fig. 13 that all block codes including

TABLE III  
COMPARISON OF SEVERAL SHORT CODES HAVING SHORTER DELAY  
( $N < 100$ ) WITH SHORT LDPC CODE

Setting Parameters:  $P_{on} = 0.3$ , SNR = -10 dB,  $N_s = 500$

Code	Rate	Optimal $P_{FA}$	$\% \eta_c$
Hamming(15,11)	0.73	0.8	65
Hamming(33,26)	0.84	0.25	55
Hamming(63,57)	0.9	0.45	39
BCH(31,21)	0.677	0.15	52
LDPC(1057,813)	0.5	0.05	60

BCH(31,21), Hamming(63,57), Hamming(31,26) and Hamming(15,11) have higher efficiency  $\eta_c$  when compared to short LDPC(96,48) code for the same value of  $P_{on} = 0.3$ . It is also clear from the figure that the Hamming code (31,26) with  $\mathbf{H}_e$  and Hamming code (63,57) with  $\mathbf{H}_e$  can achieve efficiency levels closer to the upper limit  $\eta_{max}$ . A detailed comparison of short block codes with short LDPC codes is provided in Table III.

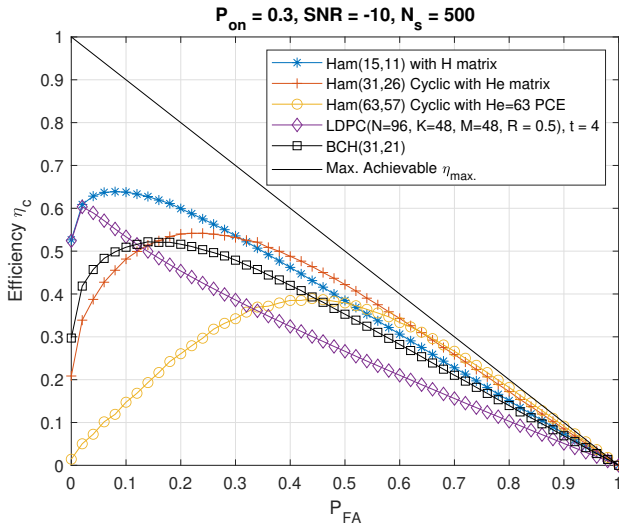


Fig. 13. Comparison of several short codes having shorter delay ( $N < 100$ ) with short LDPC code

It can be concluded by analyzing the comparison that the short LDPC codes are not always the best candidate, as they have lower erasure recovery capability for the scenario of coexistence between WiFi and NR-U. The short block codes are preferable for erasure recovery in the region where  $P_{FA} > 0.5$  under low collision rate.

### C. Comparison of concatenated codes with LDPC codes

To generate more powerful codes with less decoding complexity, we have designed two new concatenated and product codes, namely HammingSPC (Hamming  $\times$  SPC) and Product Hamming (Hamming  $\times$  Hamming) and compared them with several LDPC codes of similar lengths. It can be noticed from Fig. 14 that the efficiency  $\eta_c$  achieved with HammingSPC(1575,1368) is comparable with the achieved efficiency  $\eta_c$  using LDPC(1908,8889) which is closer to the

TABLE IV  
COMPARISON OF PRODUCT AND CONCATENATED CODES WITH LDPC CODES

Setting Parameters:  $P_{on} = 0.3$ , SNR = -10 dB,  $N_s = 500$

Code	Rate	Optimal $P_{FA}$	$\% \eta_c$
LDPC(1908)	0.889	0.42	52
HammingSPC(1550,1274)	0.82	0.35	52
HammingSPC(1575,1368)	0.87	0.45	48
ProductHamming(961,676)	0.84	0.12	70

$\eta_{max}$ . In this particular case it may be more practical to use HammingSPC(1575,1368) due to the inherent advantage of concatenation. The comparison of various concatenated codes with LDPC codes is given in Table IV.

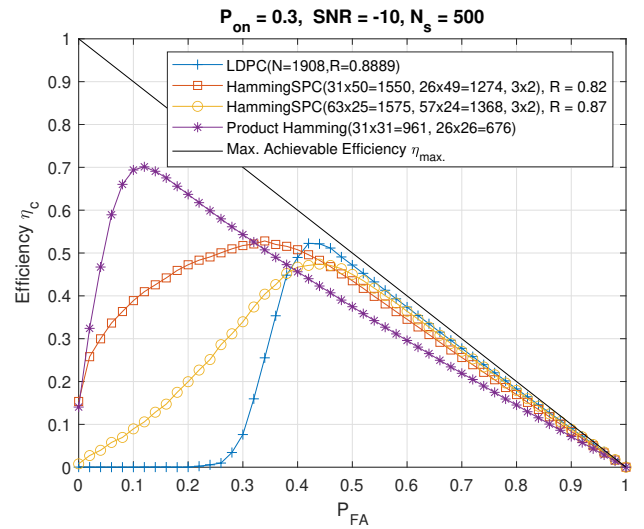


Fig. 14. Comparison of Product Codes with LDPC codes

The advantages of using product or concatenated codes were discussed in section III. Furthermore, the analysis shows that Product Hamming ( $31 \times 31 = 961, 26 \times 26 = 676$ ) provides the highest efficiency  $\eta_c = 70\%$  when  $P_{FA} = 0.1$ .

The erasure recovery capability of the product Hamming can be significantly improved with iterative decoding. Therefore, it is more practical to use concatenated or product codes when there are higher collisions as these codes achieve higher efficiency  $\eta_c$  with reduced decoding complexity. We further proved through simulation that product codes are preferable over the capacity achieving LDPC codes with reduced delay.

### D. Global network throughput and failure rate probability with multiple numbers of users

The global network throughput ( $S$ ) of CSMA/CA-based MAC protocol for WiFi STA and 5G UE, can be calculated as

$$S = \frac{U}{B+I}, \quad (27)$$

where  $U$  is the successful transmission time of users,  $B$  denotes a busy period of the channel and  $I$  is the idle period

of the channel. Equation (27) can further be written as

$$S = \frac{N_{OK}}{N_{OK}(\text{DIFS+SIFS+BO}+T_p) + N_{NOK}(\text{DIFS+SIFS+BO}+T_p)}, \quad (28)$$

where  $N_{OK}$  = number of successfully received packets,  $N_{NOK}$  = number of erroneous packets,  $T_p$  = total time for transmitting a packet. In this section, the global throughput is estimated in packets/sec, when there are multiple users attempting to access the channel within a coexistence set-up. The backoff time is a variable that depends on the number of users contending for the channel. Our simulation is set by selecting a backoff time (BO) =  $60\mu$  sec, and we further reduce this time down to 32, allowing more collisions and reducing the contention window for backoff. Note that, most of the collisions can be recoverable using erasure correcting codes without retransmission of packets. In Fig. 15, we display the global throughput given a backoff time =  $60\mu$  sec for multiple users. It is clear that the throughput is initially higher when there are a few users in contention and as the number of users increases, the global throughput starts decreasing. The blue curve shows the global throughput of the system without encoding (Uncoded CSMA/CA indicates the throughput without consideration of errors, limited only by the number of subbands). The global throughput decreases by 29% (or from 4500 to 3200) as the number of users climbs from 2 to 50. The other curves are plotted using various erasure correcting codes (by adding redundancy), showing that the maximum achieved throughput is slightly lower than the throughput achieved without coding, albeit with various packets erased due to collisions.

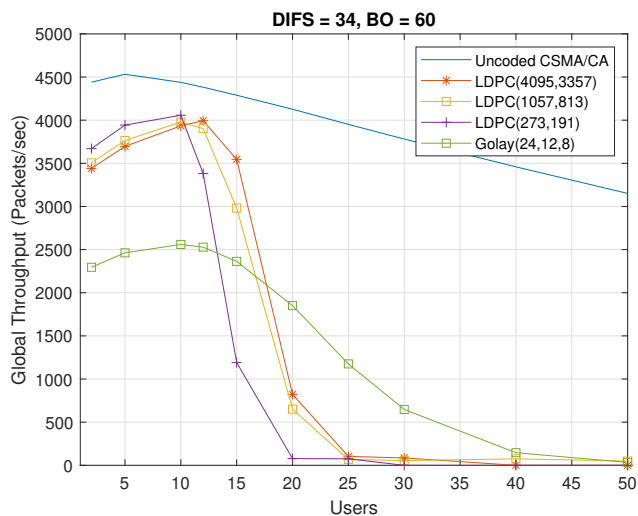


Fig. 15. Global network throughput using various codes, considering a multiple numbers of users (WiFi and 5G) with backoff =  $60\mu$  seconds.

The collisions and residual erasure probability curves are shown in Fig. 16, when BO =  $60\mu$  sec. We can see from the figure that there is a point of maximum throughput with zero packet loss as erasure recovery is performed at the receiver side [52]. The collisions will increase as the backoff time is cut down to BO =  $60\mu$  sec, while varying the number of users

from 1 to 50, inducing more access to the channel and a higher probability of collisions.

Reliability is specified by the failure probability which is defined as the probability of residual when decoding fails as described in equation (1b). Using failure probability as a measure of reliability was frequently adopted in the literature, see for example [53] and [54]. Low failure probability indicates that over a period of time, adequate lost packets in transmission are recovered using error correcting codes, guaranteeing reliable communication. High failure probability indicates otherwise. It is clear that the failure probability of LDPC(4095,3357) remains at zero and all erased packets are recovered, up to the point when we have 12 users and the collision probability was 10%. Less powerful codes (e.g., LDPC(1057,813), Golay(24,12,8)) can be used when the number of contending users is low, as shown in the figure. In addition, more powerful codes are required if the number of users is further increased to recover all erasures, lowering latency as we do not require re-transmission of packets.

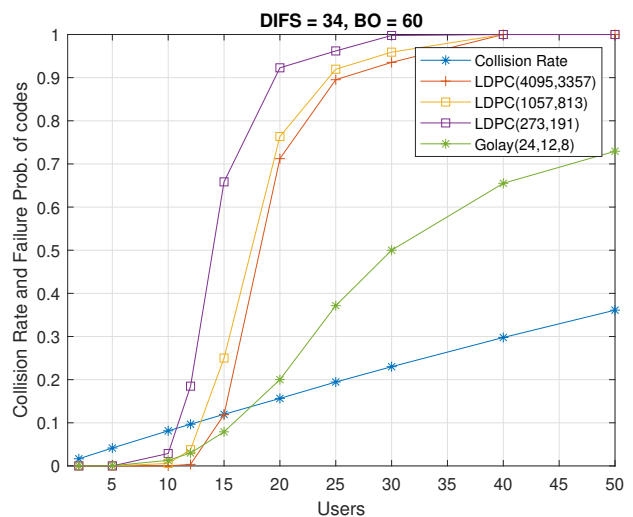


Fig. 16. Collision and failure probability of various codes considering a multiple numbers of users (WiFi and 5G) with backoff =  $60\mu$  seconds.

Similarly, the global throughput is estimated when BO =  $32\mu$  sec for multiple users. It is clear from Fig. 17 that the throughput is initially higher when there are few secondary users. And as the number of users increases, the global throughput starts decreasing. The blue curve shows the global throughput of the network without encoding. The global throughput is decreased by 56 % (or from 4500 to 2000) as the users increase from 2 to 50. The curves are plotted using various erasure correcting codes (by adding redundancy), showing that the optimal achieved throughput is a little lower than the throughput achieved without coding but with various packets erased due to collisions among multiple access attempts.

The collisions and residual erasure probability curves are shown in Fig. 18 when BO =  $32\mu$  sec. We can see from the figure that there is a point of maximum throughput with zero packet loss as erasure recovery is performed at the receiver side. The collisions will increase as the backoff time is cut

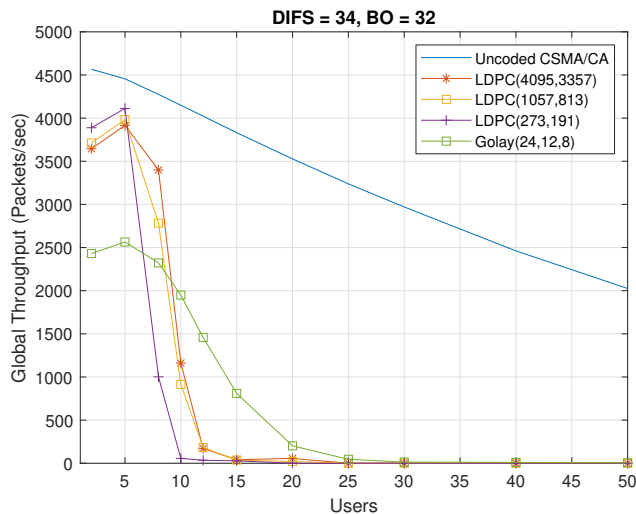


Fig. 17. Global network throughput using various codes, considering a multiple numbers of users (WiFi and 5G) with backoff =  $32\mu$  seconds.

down to  $BO = 32\mu$  sec, while varying the number of users from 1 to 50, inducing more access to the channel and a higher probability of collisions.

The failure probability of LDPC(4095,3357) remains at zero and all erased packets are recovered, up to the point when we have 5 users and the collision probability was 8%. Less powerful codes (e.g., LDPC(1057,813), Golay(24,12,8)) can be used when the number of contending users is low, as shown in Fig. 18.

## VI. ACKNOWLEDGMENT

This work was funded by the Department for Digital, Culture, Media Sport (DCMS), United Kingdom, as part of the 5G Connected Forest (5GCF) Project under its 5G Testbeds and Trials Program.

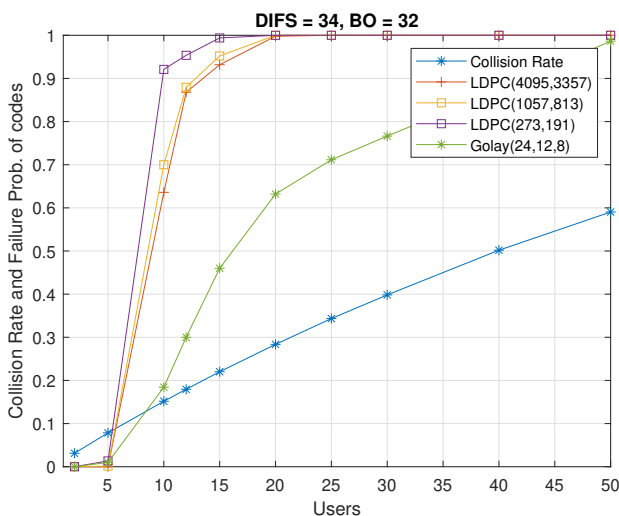


Fig. 18. Collision and failure probability of various codes considering a multiple numbers of users (WiFi and 5G) with backoff =  $32\mu$  seconds.

## VII. CONCLUSION

In this paper, we assessed the performance of various short erasure correcting codes with long codes to address the challenge of increased collisions in 5G NR-U and WiFi coexistence. We showed that our proposed codes are highly efficient for erasure recovery, especially in delay-sensitive applications. We also proposed the use of the product or concatenated codes whose decoding complexity is much simpler than long LDPC codes. A metric (efficiency  $\eta_c$ ) is introduced to compare various codes fairly by changing their parameters in the same channel characterized for a given value of  $P_{on}$ . The main objective is to find the optimum functioning point on the Receiver Operating Characteristics (ROC) curve for the sensing stage that corresponds to a trade-off among accessing channel, collisions and choice of erasure code. The channel access will depend on the parameter  $P_{FA}$ , the collision rate will depend on the parameter  $P_{ND}$ , while the choice of erasure code will impact erasure recovery.

Detailed comparisons showed that the concatenated and product codes such as Product of Hamming, or Hamming  $\times$  SPC codes provide better performance and less decoding complexity compared to various LDPC codes. These codes have a very simple decoding scheme for the component codes, and their performance is further increased through an iterative decoding process. The use of cyclic codes with the extended parity check matrix ( $\mathbf{H}_e$ ) shows a significant improvement in terms of the performance of erasure recovery and results in higher achievable efficiency  $\eta_c$ . We will further explore Polar codes in our future work and will compare their performance and decoding complexity with other short block codes.

## REFERENCES

- [1] M. Hirzallah, M. Krunz, B. Kecioğlu, and B. Hamzeh, "5G new radio unlicensed: Challenges and evaluation," *IEEE Transactions on Cognitive Communications and Networking*, pp. 1–1, 2020.
- [2] S. Lagen, L. Giupponi, S. Goyal, N. Patriciello, B. Bojovic, A. Demir, and M. Beluri, "New radio beam-based access to unlicensed spectrum: Design challenges and solutions," *IEEE Communications Surveys & Tutorials*, vol. 22, no. 1, pp. 8–37, 2020.
- [3] 3GPP, "NR-Based access to unlicensed spectrum (NR-U)," 2020. [Online]. Available: <https://www.3gpp.org/release-16>
- [4] E. Pateromichelakis, O. Bulakci, C. Peng, J. Zhang, and Y. Xia, "LAA as a key enabler in slice-aware 5G RAN: Challenges and opportunities," *IEEE Communications Standards Magazine*, vol. 2, no. 1, pp. 29–35, Mar. 2018.
- [5] M. Hirzallah, Y. Xiao, and M. Krunz, "MatchMaker: An inter-operator network sharing framework in unlicensed bands," in *2019 16th Annual IEEE International Conference on Sensing, Communication, and Networking (SECON)*. IEEE, Jan 2019.
- [6] J. Oh, Y. Kim, Y. Li, J. Bang, and J. Lee, "Expanding 5G new radio technology to unlicensed spectrum," in *2019 IEEE Globecom Workshops (GC Wkshps)*. IEEE, Dec. 2019.
- [7] Q. Cui, Y. Gu, W. Ni, and R. P. Liu, "Effective capacity of licensed-assisted access in unlicensed spectrum for 5G: From theory to application," *IEEE Journal on Selected Areas in Communications*, vol. 35, no. 8, pp. 1754–1767, Aug. 2017.
- [8] H. Song, Q. Cui, Y. Gu, G. L. Stuber, Y. Li, Z. Fei, and C. Guo, "Cooperative LBT design and effective capacity analysis for 5G NR ultra dense networks in unlicensed spectrum," *IEEE Access*, vol. 7, pp. 50 265–50 279, 2019.
- [9] V. Mushunuri, B. Panigrahi, H. K. Rath, and A. Simha, "Fair and efficient listen before talk (LBT) technique for LTE licensed assisted access (LAA) networks," in *2017 IEEE 31st International Conference on Advanced Information Networking and Applications (AINA)*. IEEE, Mar. 2017.

- [10] M. Schwartz and A. Vardy, "On the stopping distance and the stopping redundancy of codes," *IEEE Trans. Information theory*, vol. 52, no. 3, pp. 922–932, 2006.
- [11] M. Mehmouh, V. Sathya, S. Roy, and M. Ghosh, "Analytical modeling of Wi-Fi and LTE-LAA coexistence: Throughput and impact of energy detection threshold," *IEEE/ACM Transactions on Networking*, vol. 26, no. 4, pp. 1990–2003, Aug. 2018.
- [12] Y. Li, F. Baccelli, J. G. Andrews, T. D. Novlan, and J. C. Zhang, "Modeling and analyzing the coexistence of Wi-Fi and LTE in unlicensed spectrum," *IEEE Transactions on Wireless Communications*, vol. 15, no. 9, pp. 6310–6326, Sep. 2016.
- [13] A. Karim Ajami and H. Artail, "On the modeling and analysis of uplink and downlink IEEE 802.11ax Wi-Fi with LTE in unlicensed spectrum," *IEEE Transactions on Wireless Communications*, vol. 16, no. 9, pp. 5779–5795, Sep. 2017.
- [14] A. Mbengue and Y. Chang, "Performance analysis of LAA / Wi-Fi coexistence: Stochastic geometry model," Apr. 2018.
- [15] X. Wang, T. Q. S. Quek, M. Sheng, and J. Li, "Throughput and fairness analysis of Wi-Fi and LTE-U in unlicensed band," *IEEE Journal on Selected Areas in Communications*, pp. 1–1, 2016.
- [16] M. Iqbal, C. Rochman, V. Sathya, and M. Ghosh, "Impact of changing energy detection thresholds on fair coexistence of wi-fi and lte in the unlicensed spectrum," in *2017 Wireless Telecommunications Symposium (WTS)*. IEEE, 2017, pp. 1–9.
- [17] A. K. Bairagi, N. H. Tran, W. Saad, Z. Han, and C. S. Hong, "A game-theoretic approach for fair coexistence between lte-u and wi-fi systems," *IEEE Transactions on Vehicular Technology*, vol. 68, no. 1, pp. 442–455, 2018.
- [18] A. K. Bairagi, S. F. Abedin, N. H. Tran, D. Niyato, and C. S. Hong, "Qoe-enabled unlicensed spectrum sharing in 5g: A game-theoretic approach," *IEEE Access*, vol. 6, pp. 50 538–50 554, 2018.
- [19] P. Campos, Á. Hernández-Solana, and A. Valdovinos-Bardají, "Analysis of hidden node problem in LTE networks deployed in unlicensed spectrum," *Computer Networks*, vol. 177, p. 107280, 2020.
- [20] T. A. Atif, A. M. Baswade, B. R. Tamma, and A. A. Franklin, "A complete solution to LTE-U and Wi-Fi hidden terminal problem," *IEEE Transactions on Cognitive Communications and Networking*, vol. 5, no. 4, pp. 920–934, 2019.
- [21] S. Liu, R. Yin, and G. Yu, "Hybrid adaptive channel access for LTE-U systems," *IEEE Transactions on Vehicular Technology*, vol. 68, no. 10, pp. 9820–9832, 2019.
- [22] Z. Qin, A. Li, and H. Wang, "A cournot game approach in the duty cycle in csat algorithm for Wi-Fi/LTE-U coexistence," in *2020 International Conference on Wireless Communications and Signal Processing (WCSP)*. IEEE, 2020, pp. 1076–1081.
- [23] P. Campos, Á. Hernández-Solana, and A. Valdovinos-Bardají, "Machine learning for hidden nodes detection in unlicensed LTE networks," *Computer Networks*, p. 108862, 2022.
- [24] V. Sathya, M. I. Rochman, and M. Ghosh, "Hidden-nodes in coexisting laa & wi-fi: a measurement study of real deployments," in *2021 IEEE International Conference on Communications Workshops (ICC Workshops)*. IEEE, 2021, pp. 1–7.
- [25] —, "Measurement-based coexistence studies of laa & wi-fi deployments in chicago," *IEEE Wireless Communications*, vol. 28, no. 1, pp. 136–143, 2020.
- [26] M. Luby, "LT codes," in *Foundations of Computer Science, 2002. Proceedings. The 43rd Annual IEEE Symposium on*, 2002, pp. 271–280.
- [27] M. Luby, T. Gasiba, T. Stockhammer, and M. Watson, "Reliable multimedia download delivery in cellular broadcast networks," *IEEE Transactions on Broadcasting*, vol. 53, no. 1, pp. 235–246, Mar. 2007.
- [28] A. Shokrollahi, "Raptor codes," *IEEE Trans. Information Theory*, vol. 52, no. 6, pp. 2551–2567, 2006.
- [29] A. Muqabel, "Enhanced upper bound for erasure recovery in spc product codes," *ETRI journal*, vol. 31, no. 5, 2009.
- [30] M. A. Kousa and A. H. Muqabel, "Cell loss recovery using two-dimensional erasure correction for ATM networks," *7th International Conference on Telecommunication Systems Modeling and Analysis*, March 1999.
- [31] J. H. Bae, A. Abotabl, H.-P. Lin, K.-B. Song, and J. Lee, "An overview of channel coding for 5g nr cellular communications," *APSIPA Transactions on Signal and Information Processing*, vol. 8, 2019.
- [32] T. Rosenqvist and J. Sloof, "Implementation and evaluation of polar codes in 5g," 2019.
- [33] I. Tal and A. Vardy, "List decoding of polar codes," *IEEE Transactions on Information Theory*, vol. 61, no. 5, pp. 2213–2226, 2015.
- [34] P. Trifonov and V. Miloslavskaya, "Polar subcodes," *IEEE Journal on Selected Areas in Communications*, vol. 34, no. 2, pp. 254–266, 2015.
- [35] P. Trifonov and G. Trofimiuk, "A randomized construction of polar subcodes," in *2017 IEEE International Symposium on Information Theory (ISIT)*. IEEE, 2017, pp. 1863–1867.
- [36] Y. Ma and D. G. Kuester, "Mac-layer coexistence analysis of LTE and WLAN systems via listen-before-talk," in *2017 14th IEEE Annual Consumer Communications & Networking Conference (CCNC)*. IEEE, 2017, pp. 534–541.
- [37] B. Reynders, W. Meert, and S. Pollin, "Range and coexistence analysis of long range unlicensed communication," in *2016 23rd International Conference on Telecommunications (ICT)*. IEEE, 2016, pp. 1–6.
- [38] S. Sagari, I. Seskar, and D. Raychaudhuri, "Modeling the coexistence of LTE and WiFi heterogeneous networks in dense deployment scenarios," in *2015 IEEE international conference on communication workshop (ICCW)*. IEEE, 2015, pp. 2301–2306.
- [39] S. Sagari, S. Baysting, D. Saha, I. Seskar, W. Trappe, and D. Raychaudhuri, "Coordinated dynamic spectrum management of LTE-U and Wi-Fi networks," in *2015 IEEE International Symposium on Dynamic Spectrum Access Networks (DySPAN)*. IEEE, 2015, pp. 209–220.
- [40] G. Naik, J. Liu, and J.-M. J. Park, "Coexistence of dedicated short range communications (dsrc) and Wi-Fi: Implications to Wi-Fi performance," in *IEEE INFOCOM 2017-IEEE Conference on Computer Communications*. IEEE, 2017, pp. 1–9.
- [41] Y. Gao, X. Chu, and J. Zhang, "Performance analysis of LAA and WiFi coexistence in unlicensed spectrum based on markov chain," in *IEEE Global Communications Conference (GLOBECOM)*. IEEE, Dec. 2016.
- [42] J. Liu, Q. Cui, J. Zhang, W. Ni, Z. Fei, and Y. Li, "Tradeoff between reliability and channel utilization efficiency for 5G NR in unlicensed spectrum," 2019.
- [43] M. Wellens, J. Riihijärvi, and Mähönen, "Modelling primary system activity in dynamic spectrum access networks by aggregated on/off-processes," in *Proc. of 4th IEEE Workshop on Networking Technologies for SDR Networks*, Jun. 2009.
- [44] M. S. Afaqui, E. Garcia-Villegas, and E. Lopez-Aguilera, "Ieee 802.11 ax: Challenges and requirements for future high efficiency WiFi," *IEEE wireless communications*, vol. 24, no. 3, pp. 130–137, 2016.
- [45] M. Wellens, J. Riihijärvi, and P. Mähönen, "Empirical time and frequency domain models of spectrum use," *Physical Communication*, vol. 2, no. 1–2, pp. 10–32, Mar. 2009.
- [46] C. Tellambura, "Spectrum sensing methods and their performance," in *Handbook of Cognitive Radio*. Springer Singapore, 2019, pp. 163–184.
- [47] P. Tortelier and M. Azeem, "Improving the erasure recovery performance of short codes for opportunistic spectrum access," *WPMC*, 2011.
- [48] J. Van Wousterghem, A. Alloum, J. J. Boutros, and M. Moeneclaey, "On short-length error-correcting codes for 5G-NR," *Ad Hoc Networks*, vol. 79, pp. 53–62, 2018.
- [49] Q.-Y. Yu, T. Li, H.-R. Lin, and F.-F. Cao, "Parity-check coding transmit diversity for wireless communications with high mobility," *IEEE Transactions on Vehicular Technology*, 2021.
- [50] S. Kay, *Fundamentals of Statistical Signal Processing: Detection Theory*. Prentice-Hall, 1998.
- [51] L. Rugini, P. Banelli, and G. Leus, "Small sample size performance of the energy detector," *IEEE Communications Letters*, vol. 17, no. 9, pp. 1814–1817, 2013.
- [52] M. Karzand, D. J. Leith, J. Cloud, and M. Médard, "Design of fec for low delay in 5G," *IEEE Journal on Selected Areas in Communications*, vol. 35, no. 8, pp. 1783–1793, 2017.
- [53] B. Chen and F. M. Willems, "Secret key generation over biased physical unclonable functions with polar codes," *IEEE Internet of Things Journal*, vol. 6, no. 1, pp. 435–445, 2018.
- [54] J. Sachs, G. Wikstrom, T. Dudda, R. Baldemair, and K. Kittichokechai, "5g radio network design for ultra-reliable low-latency communication," *IEEE network*, vol. 32, no. 2, pp. 24–31, 2018.



**M. Moazam Azeem** is currently working as Assistant Professor at College of Computer Science and Engineering, Department of Computer Engineering, Qatar University. He was working as Researcher at School of Computing and Digital Technology, Birmingham City University, UK, in 2021. He worked as a System Architect at Continental Automotive Services, France, at department of Wireless Communication from 2018-2020. He was Research Associate from 2015-2018 at Sorbonne University, Paris.

Moazam received his PhD degree in Radiocommunications from France-Telecom in collaboration with CNAM Paris in 2014. He received his Master's degree in System on Chip design from KTH, Stockholm, Sweden in 2010 and got his Bachelor's degree in electrical engineering from UET Taxila in 2007. He is also the inventor of a Patent in reliable data transmission for multiple users in cellular communication. His main research interests lie in Cognitive Radios, Spectrum Sensing, Opportunistic Spectrum Access, Erasure Correcting codes, dependable fault tolerant computing and Multiple FPGA Boards. He Contributed to FP7 European project that was started by European Commission with budget of 8.1€ billion. He also contributed to Industrial project Flex at Orange Labs, WinNoCod and WasgaServe projects at Sorbonne University.



**Raouf Abozariba** (S'16 - M'17) received the MSc degree in electronics engineering and the PhD degree in the area of wireless communications from Staffordshire University in 2008 and 2017, respectively. He was a senior research associate at Lancaster University from 2018 to 2019, where he led the monitoring element of the 5G rural integrated testbed (5GRIT) project. He joined Birmingham City University in 2019 where he is currently a Senior Lecturer, broadly working around NOMA, Channel Coding, Machine Vision, Video Streaming

and quality of service (QoS) network monitoring. From 2020 to 2022 Raouf served as a Co-Investigator on the 5G Connected Forest (5GCF) project, where AI, robots, UAVs and various networking technologies are blended together to digitise and automate health of the forest assessment in a smart and cost-effective way. He is currently leading the development of a custom-made 4G/5G real-time QoS monitoring platform, which will be utilised to survey Nottinghamshire County in the coming months, through a project managed by Nottingham County Council and funded by Local Government Association, UK. Raouf is also an active member of the IEEE and has published many technical papers in reputed scientific journals and international conferences in the area of communications.



**Taufiq Asyhari A. Taufiq Asyhari** received the BEng (Hons) degree in Electrical and Electronic Engineering from Nanyang Technological University, Singapore, in 2007, and the PhD degree in Information Engineering from the University of Cambridge, UK, in 2012. He is currently an Associate Professor (equivalent to Reader) in Networks and Communications at Birmingham City University, UK. He has been an Academic Visitor at Cranfield University, UK, and Telkom University, Indonesia. He previously held full-time/visiting positions at National

Chiao Tung University, Bell Laboratories, and the University of Stuttgart. His research interests include the areas of information theory, communication and coding theory, and signal processing techniques with applications to wireless and molecular communication networks, the Internet of Things, and data analytics. Dr Asyhari is a Fellow of the Higher Education Academy, UK and Senior Member of IEEE. He has served as a member of the Editorial Board and the Technical Program Committee in numerous leading international journals and conferences. He is currently the Academic Lead for the multi-million pound 5G Connected Forest project funded by the UK DCMS. He received the notable Samsung Global Research Outreach Award, in 2017, the Silver Medal at the International Trade Fair iENA 2017, the IEEE-EURASIP Best Paper Award at ISWCS 2014, the National Science Council of Taiwan Starting Grant, in 2013, and the Cambridge Trust - Yousef Jameel Scholarship.